Template-Assisted Fabrication of Salt-Independent Catalytic Tubular Microengines

Kalayil Manian Manesh, Maria Cardona, Rodger Yuan, Michael Clark, Daniel Kagan, Shankar Balasubramanian, and Joseph Wang*

Department of Nanoengineering, University of California San Diego, La Jolla, California 92093

ARTICLE

ABSTRACT A simplified template-assisted layering approach for preparing catalytic conical tube microjet engines based on sequential deposition of platinum and gold on an etched silver wire template followed by dicing and dissolution of the template is described. The method allows detailed control over the tube parameters and hence upon the performance of the microengine. The recoiling bubble propulsion mechanism of the tubular microengine, associated with the ejection of internally generated oxygen microbubbles, addresses the ionic-strength limitation of catalytic nanowire motors and leads to a salt-independent movement. Similar rates of bubble generation and motor speeds are observed in salt-free and salt-rich media (at elevated ionic-strength environments as high as 1 M NaCl). Plating of an intermediate nickel layer facilitates a magnetically guided motion as well as the pickup and transport of large (magnetic) "cargo". Surfactant addition is shown to decrease the surface tension and offer a more frequent formation of dense smaller bubbles. The new and improved motor capabilities along with the simple preparation route hold great promise for using catalytic micromotors in diverse and important applications.

KEYWORDS: catalytic motor · microcone · propulsion · bubble recoil · salt

Locomotion of nanoscale objects through fluid environments is one of the major exciting and challenging areas of nanotechnology.[1,2] The remarkable performance of biomotors has inspired scientists to build up synthetic nanomachines that mimic these natural counterparts by using catalytic reactions to create forces based on chemical gradients. Recently, particular attention has been given to chemically powered catalytic motors that exhibit autonomous self-propulsion in the presence of hydrogen peroxide fuel.[2−4] Most commonly, such catalytic nanomotors rely on the electrochemical propulsion of bimetal (Au/Pt, Au/Ni) nanowires through an electrokinetic self-electrophoresis mechanism.[5] Such propulsion mechanism implies that chemically powered catalytic nanomotors can operate only in low ionic-strength aqueous solutions, as the their axial velocity decreases linearly with the solution conductivity.[6] This ionic-strength limitation precludes many potential applications of catalytic nanoscale and microscale motors (particularly biomedical ones) and requires new propulsion mechanisms.

Recent efforts by Mei's team illustrated the design of a powerful catalytic rolled-up tubular microjet engine.[7] These catalytic microtubes are propelled rapidly and efficiently by a recoiling mechanism involving expelled oxygen microbubbles generated catalytically on the inner platinum surface. Such impressive performance, however, requires a top-down photolithographic fabrication route involving evaporation of multiple thin metallic layers onto a sacrificial photoresist followed by stress-assisted rolling of multilayer structure into a microtube. Such 2D patterning requires critical control over internal stresses induced by varying deposition conditions, thereby making the development of defect-free 3D roll-up structures quite challenging.

Here we report on a greatly simplified template-assisted preparation and new capabilities of conical microtube engine based sequential electrodeposition of platinum and gold layers onto an etched silver wire template, followed by dicing and dissolution of the silver wire template (Figure 1). The method allows detailed control over the tube dimensions, geometry, or materials and hence upon the performance of the microengine. The optimal motor geometry has been selected based on critical design considerations aimed at maximizing the intertial propulsion and minimizing viscous effects, and after examining different motor shapes and dimensions. As indicated from the SEM image of Figure 2B, the new template-assisted preparation route leads to well-defined bimetal conical microtubes. Such conical microtube engine design facilitates the entrance of the fuel through the small radial opening, with the catalytically generated gas bubbles traveling along

See the accompanying Perspective by Mirkovic *et al.* on p 1782.

*Address correspondence to josephwang@ucsd.edu.

Received for review January 8, 2010 and accepted March 8, 2010.

Published online March 15, 2010.
10.1021/nn1000468

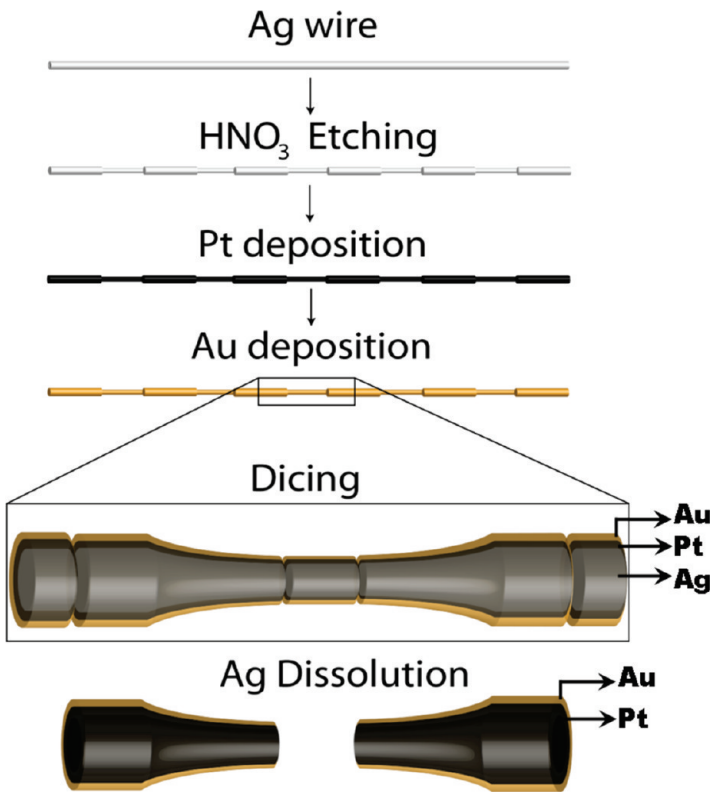

Figure 1. Schematic illustrating the steps involved in the template-assisted preparation of the tubular microcone engine. This scheme depicts a visual understanding of the silver template preparation, electroplating of the Pt and Au layers, dicing of the coated wire, and dissolution of the silver template. Nitric acid dissolves the silver wire, creating concave geometry, which remains when Pt and Au are electroplated.

a sloped transition and ejecting out from a larger radial opening to generate the force propelling the engine (Figure 2C). The oxygen-bubble propulsion mechanism of the tubular microjet engine addresses the ionic-strength limitation of catalytic nanowire motors and allows salt-independent movement (including high-speed propulsion in very high ionic-strength medium of one molar salt). Magnetically directed movement and transport of heavy cargo are accomplished through the deposition of an intermediate nickel layer. Such design considerations, template-assisted motor fabrication, salt-independent propulsion, cargo pickup and transport, and other attractive performance characteristics are discussed in the following sections.

RESULTS AND DISCUSSION

Here we illustrate the template-assisted engineering layer approach for fabricating synthetic bubble-propelled micromotors and their efficient propulsion in high ionic-strength media. Such chemically powered motors were prepared by plating a catalytic platinum surface onto predefined silver wire templates. A gold outerlayer was used to prevent bubble formation on the external surface. Some experiments involved an intermediate nickel layer for magnetic navigation and cargo transport. Figure 2 shows SEM images of the etched Ag wire (A) and of the resulting Pt−Au tubular microcone (B). The nitric acid treatment led to the etching of the cylindrical silver wire into a concave microcone. The exact length and dimensions of the microcone are controlled by the dicing step (Supporting Information Figure 1), while the degree of concavity is controlled by the etching conditions (such as etching time and concentration of nitric acid). The conical shape of the wire template (after the nitric acid etching) is clearly indicated from Figure 2A. Such concave geometry curvature minimizes the turbulent flow inside the micromotor and provides a favorable gradient for forward propulsion.[7] It also increases efficiency of the oxygen-bubble production and the overall controlled fluid flow. Figure 2B displays an image of the open tubular microcone after dissolution of the silver template. The nitric acid etching resulted in a smoothed internal Pt surface, along with a rough external gold surface (associated with the electrodeposition of the gold). Figure 2C displays the conceptualized diagram of the recoil propulsion mechanism of a microcone engine. The peroxide fuel enters the microcones through the small radial opening, and its electrocatalytic decomposition on the inner platinum surface produces oxygen gas that nucleates into bubbles. These oxygen bubbles travel along a sloped transition and exit through the larger open-

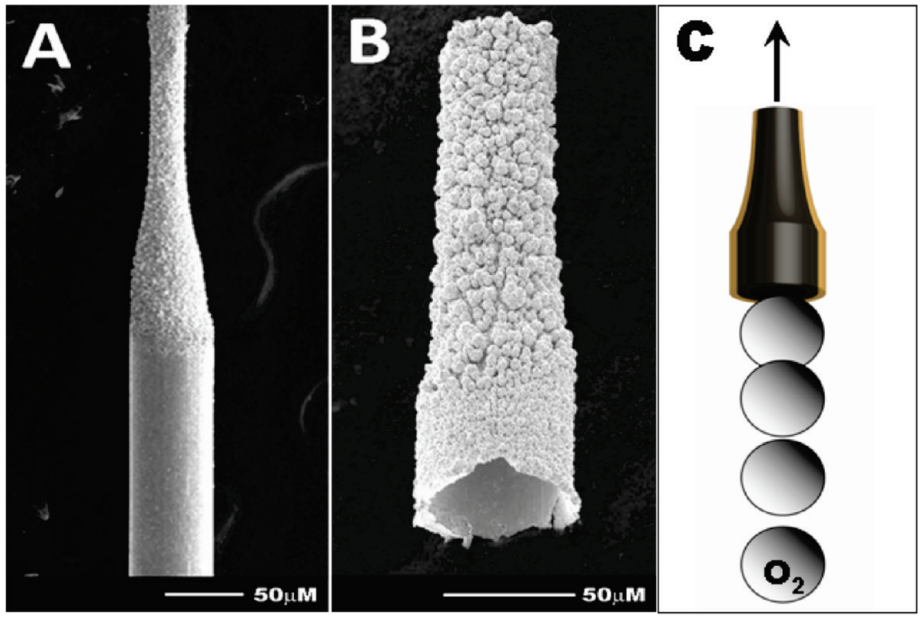

Figure 2. SEM images of the (A) etched 50 μm diameter Ag wire, (B) Pt−Au tubular microcone following the Ag dissolution, and (C) oxygen microbubbles, generated electrocatalytically on the inner platinum surface, are ejected from the larger opening of the microcone and propel the motor.

ing of the microcone (due to the pressure differential caused by the asymmetry of the size of the inlet and outlet openings), producing a force in the opposite direction of the bubble ejection and resulting in axial movement of the microcone body.

Figure 3 displays time-lapse images for the movement of the tubular microcone engine in a 15% peroxide solution over a 2 s period at 0.4 s intervals. These images illustrate a tail of microbubbles (~100 μm diameter) catalytically generated on the inner surface and released from the rear of the microcone at a rate of 10 bubbles/s. Such ejection of bubbles from the larger opening of the microcone propels the jet engine forward at a speed of around 456 μm/s (corresponding to around three body lengths/s). The fast production of small bubbles and steady motor propulsion are clearly illustrated in the corresponding video (Supporting Information video 1). Lowering the peroxide fuel concentration resulted in decreased bubble frequency and a slower motor speed of 186 μm/s in 5% H_2O_2 (not shown).

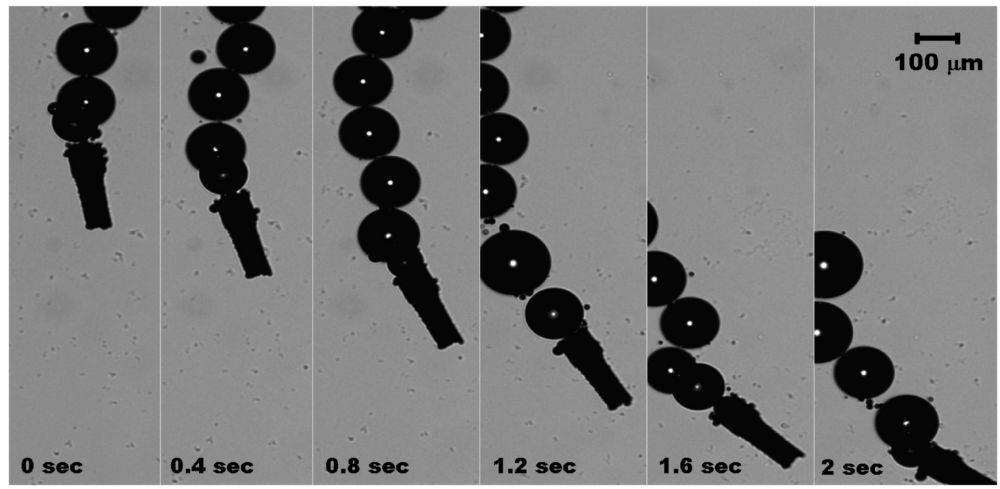

Figure 3. Chemically powered Pt−Au tubular microcone: time-lapse images for the movement of the tubular engine rocket in 15% hydrogen peroxide over a 2 s period at 0.4 s intervals. Oxygen bubbles are ejected from the larger opening side.

Catalytic nanowire motors commonly operate only in low ionic-strength aqueous solutions and hence cannot be applied in many relevant environments.[6] The oxygen-bubble propulsion mechanism of the tubular microjet engine addresses this ionic-strength limitation and can expand the scope of artificial nanomotors to salt-rich environments. Supporting Information video 2 compares the movement of the catalytic tubular microcone motor in the absence (A) and presence (B) of 1 M NaCl. The time-lapse images of the motion in this salt-rich environment (shown in Figure 4) indicate high rate of bubble generation and a motor speed of 183 μm/s in 5% H_2O_2 (similar to the 186 μm/s speed observed in salt-free conditions). Apparently, and as expected from the bubble-propulsion mechanism, the high ionic-strength medium (up to 1 M) has affected the propulsion of microtube engines by merely 1−3% (Supporting Information Figure 2). Such minimal salt effect has important implications upon the scope of future applications of catalytic motors.

The geometry and dimensions of the silver wire template have a profound effect upon the performance of the new micromotors. Optimization was carried out by varying the silver wire templates, through changes in its shape, diameter, length, or surface chemistry. The new method allows also detailed control over the tube materials. Preliminary experiments involved the use of a polymeric polypyrrole (PPy) outer layer instead of gold. The resulting microtubes, however, yielded bubble generation from the external surface because of the porous nature of PPy. The incorporation (deposition) of an intermediate nickel layer will be discussed below (in connection to magnetic pickup of cargo). Various geometries of tubular micromotors (cylindrical, step cone, and smooth cone) were examined in connection to different diameters of the silver wire template (ranging from 25 to 100 μm). The most favorable propulsion was observed for Pt−Au tubular microcones in connection to 50 μm wire templates. Design considerations included the study of flow losses in single-phase duct flow of stepped and coned tubular geometries. Trials with straight duct, stepped cone, and smooth cone designs—with different inlet/outlet area ratios—yielded positive results but lacked the desired speed and control. The concave hyperbolic-shaped cone (of Figures 1 and 2) surpassed the other designs in performance by maximizing the amount of recoil that gets translated into forward mo-

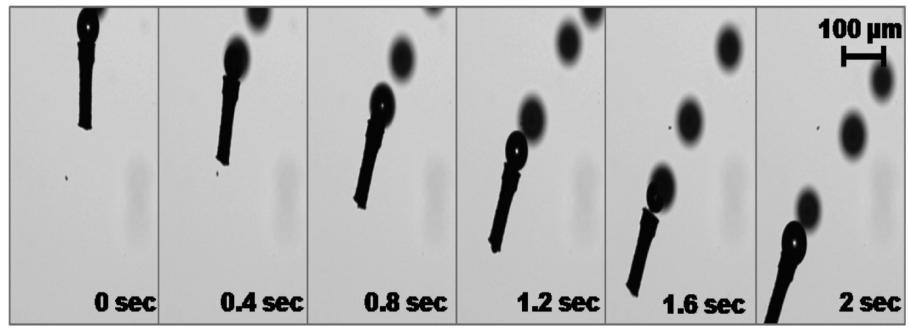

Figure 4. Movement of the Pt−Au tubular microcone engine in the presence of 1 M sodium chloride (containing 5% hydrogen peroxide). Time-lapse images over a 2 s period at 0.4 s intervals.

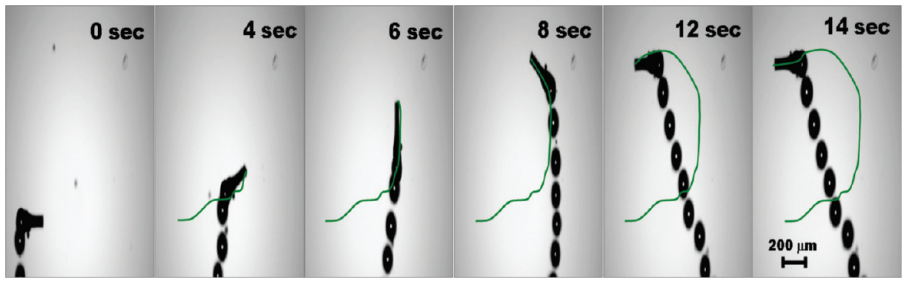

Figure 5. Magnetically guided movement of a Pt−Ni−Au tubular microcone: time-lapse images over a 14 s period revealing a defined shaped motion in the presence of 5% hydrogen peroxide.

tion. This smooth cone geometry displayed a more streamlined efflux of bubbles, a higher bubble-formation frequency, and hence an enhanced micromotor speed and power compared to other geometries of microtube engines, and that was thus used for all subsequent work. Such design avoids the sudden pressure drop or bubbles evolving from both sides characterizing the step cone or cylindrical geometries, respectively. Variations in the inlet/outlet diameter ratios and the length/width ratio of the conical design were evaluated for optimizing the fluid's exit pressure and improving the flow pattern for optimal bubble production. Most favorable performance was obtained using a length of 150 μm and inlet and outlet diameters of 30 and 50 μm, respectively. Proper cleaning of the silver template prior to the platinum deposition led to a smooth inner platinum surface and to minimization of the head loss (experienced by the bubbles).

The new propulsion capabilities of the conical microtube engine can be coupled with a magnetically directed movement with the introduction of a magnetic metal layer. The template-assisted preparation protocol allows convenient incorporation of the magnetic layer. For this purpose, a nickel layer can be readily electroplated on top of the platinum layer and subsequently coated with an external electroplated gold layer. The ability to use magnetic control to guide the motion of the Pt−Ni−Au tubular microjet engine is illustrated in Figure 5. This figure displays time-lapse images during the magnetically guided U-shaped movement of the conical microtube over a 14 s period (Supporting Information video 3). The incorporation of a ferromagnetic Ni layer into the microcone enabled a magnetic remote control and guidance in the preselected U-shaped route. Such guided motion is accomplished without compromising the engine speed.

Controlled motion and cargo transport and manipulation capabilities along predetermined paths within microfluidic channels represent a critical step toward designing integrated microdevices for a wide range of applications, including separation, enrichment, or assembly. Such capabilities were illustrated before in connection to catalytic nanowire motors[8,9] but not in connection to tubular microengines. Figure 6 and the corresponding video (Supporting Information video 4) demonstrate the ability of the magnetic tubular microengine to load a spherical (100 μm diameter) cargo and transport it along predetermined paths. A guided movement of the Pt−Ni−Au microengine toward the large magnetic-sphere "cargo" is observed along with a dynamic loading of this cargo onto the propelled microtube and its transport over a predetermined path. These data also indicate that the speed of the microengine is not compromised by the cargo loading, reflecting the high propulsion power.

Surfactant (Triton X-100) addition to the fuel solution has led to a formation of dense smaller bubbles. Low concentrations of Triton X-100 were added to reduce the hydrophobic nature of the Pt layer and the surface tension to improve the Pt wetting (with the aqueous peroxide fuel solution) and reduce the possible drag caused by polar attractions between the aqueous solution and gold outer layer. The resulting surfactant-induced changes in the propulsion of the tubular microjet engine are illustrated from the time-lapse images in Supporting Information Figure 3. A long tail of small bubbles is clearly visualized. Such reduction in bubble size leads to a smaller propulsive force and to smoother propulsion (with shorter moving "steps"). Although the bubble frequency is increased (~80 bubbles/s) and more streamlined, the propulsion is greatly reduced with the microcone moving at a slower speed of around 250 μm/s in 15% H_2O_2, or *ca.* 1.5 body length/s (compared to over 450 μm/s without the surfactant). This is attributed to lower propulsion forces generated by bubbles of smaller radius compared to larger ones. This is in contrast to the microtube engines of Mei *et al.*[7]

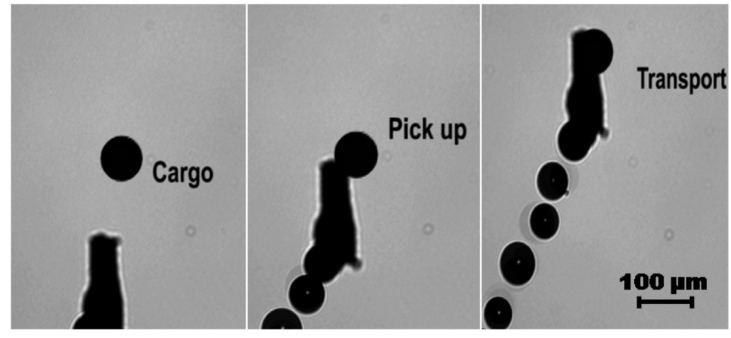

Figure 6. Sequential optical microscopy images of the dynamic loading and transport of a 100 μm diameter magnetic microparticle cargo by the Pt−Ni−Au tubular microengine in the presence of 5% hydrogen peroxide.

In conclusion, we have demonstrated a template-assisted approach for preparing chemically powered salt-independent tubular microjet engines based on sequential deposition of platinum and gold onto a conical silver wire template followed by dissolution of the template. Such template-assisted approach represents a greatly simplified protocol, compared to the top-down lithographic route used earlier for preparing rolled-up catalytic microtubes,[10] and offers a low-cost avenue to engineer tubular microjets consisting of different materials or material combinations. The oxygen-recoil propulsion mechanism of the tubular microjet engine addresses the major ionic-strength limitation of catalytic nanowire motors and allows salt-independent movement (including high-speed propulsion in a one molar salt solution). Such salt independence opens the door to a wide range of practical applications of microscale motors. Placing a ferromagnetic intermediate nickel layer facilitates a directed guided motion as well as the pickup and transport of large magnetic cargo along a predetermined path. Such new and improved capabilities of tubular microengines, along with the simple template-assisted fabrication route, indicate great potential for performing important tasks in diverse fields.

EXPERIMENTAL SECTION

Various geometries of tubular micromotors (cylindrical, step cone, and smooth cone) were examined and prepared by a sequential electrodeposition of platinum (Pt) and gold (Au) layers onto the silver microwire template (3 cm long, 50 μm diameter; Cat No. AG005110, 99.9% purity, Goodfellow, Oakdale, PA). Figure 1 shows the detailed procedure used for preparing the microcone engine. For preparing cone microtubes (Figure 1), silver microwires were initially secured under tension to an elevated platform. Concaved geometry templates were obtained by etching silver wire at evenly spaced segments with 30% nitric acid droplets (10 μL) for 30 s, followed by a thorough rinsing with distilled water. The etched silver wire template was soldered to tin-coated copper wire contact and served as a "working electrode" for the subsequent electrodeposition steps.

The following Pt−Au electrodeposition protocol was used in connection to different shapes of the silver wire template. Platinum was deposited galvanostatically at −2 mA for 240 s using a commercial platinum plating solution (Platinum RTP; Technic Inc., Anaheim, CA) along with a Pt wire counter electrode and Ag/AgCl (3 M KCl) reference electrode. Subsequently, Au was electrodeposited at −0.9 V from a gold plating solution (Orotemp 24 RTU RACK; Technic Inc.) for 200 s. The Pt−Au-coated silver wire templates were diced at desired locations using a DAD3220 Disco automatic dicing saw to create 150−300 μm long segments (Supporting Information Figure 1). The silver wire template was subsequently dissolved for 5 min using 25% (v/v) nitric acid. This process created tubular microcones with an inner platinum surface covered by an external gold layer. These tubular motors were collected by centrifugation at 2000 rpm for 2 min and washed repeatedly with nanopure water (18.2 MΩ · cm) until a neutral pH was achieved. All tubular microcones were stored in nanopure water at room temperature, and their speed was tested on the same day of synthesis. The resulting microcone tubes were tested for their movement in a aqueous solution of hydrogen peroxide fuel solution. The influence of the surfactant (Triton X-100) upon the propulsion of Pt−Au tubular microcone was studied by mixing a 15% hydrogen peroxide solution with solutions of Triton X-100 (0.1% in water) with a 1:0.1 ratio.

For magnetically directed propulsion, a nickel layer was electroplated ("sandwiched") between the platinum and gold layers. The nickel deposition proceeded for 120 s at −1.0 V using a nickel-plating solution [20 g L^{-1} $NiCl_2 \cdot 6H_2O$, 515 g L^{-1} $Ni(H_2NSO_3)_2 \cdot 4H_2O$, and 20 g L^{-1} H_3BO_3 (buffered to pH 3.4)]. In this case, the silver template was dissolved in a H_2O_2/NH_4OH (1:1) solution. The tubular motors were magnetically directed and guided by rotating the external magnet pair at ~10 cm away from the glass slide without changing the distances. Such position allows only changes of an alignment in the direction of tubular motor by a weak magnetic field. We also examined an outer layer of polypyrrole (PPy) (instead of Au) prepared by cycling the potential between 0 to 1.0 V at a scan rate of 100 mV/s using 0.5 mM pyrrole solutions containing either tetraethylammonium tetrafluoroborate in acetonitrile (*vs* a Ag/Ag^+/ACN nonaqueous reference electrode) or sodium chloride (*vs* Ag/AgCl, 3 M KCl reference electrode) in water as dopants. For cargo pickup experiments, commercially available polystyrene beads (100 μm Polysciences, Inc., Warrington, PA) were purchased and dispersed as monolayers on precleaned glass slides. The top side of the dried polystyrene was coated with a titanium layer (25 nm thick) followed by 100 nm of nickel and 200 nm of gold using an Ebeam evaporator (Temescal BJD 1800).

Images were captured using an inverted optical microscope (Nikon Instrument Inc., Eclipse TE2000-S), equipped with a 5× objective, a Photometrics CoolSnap HQ2 camera (Roper Scientific, Duluth, GA). Images were taken at a rate of 10 frames/s to create supporting videos and figures. The micromotor movement was tracked using Metamorph 7.1 software (Molecular Devices, Sunnyvale, CA). Detail explanations regarding the tracking of tubular micromotor movement using an optical microscope (Nikon Instrument Inc., Eclipse 80i, Melville, NY) were reported in our earlier literature.[10,11] The morphology of microtubes was examined by field emission scanning electron microscopy (Phillips XL30 ESEM).

Acknowledgment. This work was supported by the National Science Foundation (Award Number CBET 0853375).

Supporting Information Available: Additional figures and videos. This material is available free of charge *via* the Internet at http://pubs.acs.org.

REFERENCES AND NOTES

1. Mallouk, T. E.; Sen, A. Powering Nanorobots. *Sci. Am.* **2009**, *300*, 72–77.
2. Ozin, G. A.; Manners, I.; Fournier-Bidoz, S.; Arsenault, A. Dream Nanomachines. *Adv. Mater.* **2005**, *17*, 3011–3018.
3. Paxton, W. F.; Sundararajan, S.; Mallouk, T. E.; Sen, A. Chemical Locomotion. *Angew. Chem., Int. Ed.* **2006**, *45*, 5420–5429.
4. Wang, J. Can Man-Made Nanomachines Compete with Nature Biomotors? *ACS Nano* **2009**, *3*, 4–9.
5. Wang, Y.; Hernandez, R. M.; Bartlett, D. J.; Bingham, J. M.; Kline, T. R.; Sen, A.; Mallouk, T. E. Bipolar Electrochemical Mechanism for the Propulsion of Catalytic Nanomotors in Hydrogen Peroxide Solutions. *Langmuir* **2006**, *22*, 10451–10456.
6. Paxton, W. F.; Baker, P. T.; Kline, T. R.; Wang, Y.; Mallouk, T. E.; Sen, A. Catalytically Induced Electrokinetics for Motors and Micropumps. *J. Am. Chem. Soc.* **2006**, *128*, 14881–14888.
7. Solovev, A.; Mei, Y.; Bermdez, E.; Huang, G.; Schmidt, O. Catalytic Microtubular Jet Engines Self-Propelled by Accumulated Gas Bubbles. *Small* **2009**, *5*, 1688–1692.
8. Burdick, J.; Laocharoensuk, R.; Wheat, P.; Posner, J. D.; Wang, J. Synthetic Nanomotors in Microchannel Networks: Directional Microchip Motion and Controlled Manipulation of Cargo. *J. Am. Chem. Soc.* **2008**, *130*, 8164–8165.

9. Sundararajan, S.; Lammert, P. E.; Zudans, A. W. Catalytic Motors for Transport of Colloidal Cargo. *Nano Lett.* **2008**, *8*, 1271–1276.
10. Laocharoensuk, R.; Burdick, J.; Wang, J. CNT-Induced Acceleration of Catalytic Nanomotors. *ACS Nano* **2008**, *2*, 1069–1075.
11. Demirok, U. K.; Laocharoensuk, R.; Manesh, K. M.; Wang, J. Ultrafast Catalytic Alloy Nanomotors. *Angew. Chem., Int. Ed.* **2008**, *120*, 9489–9491.